Hybrid Structured/Unstructured Grid Computations for the F/A - 18 at High Angle of Attack

Hybrid Structured/Unstructured Grid Computations for the F/A-18 at High Angle of Attack

*Robert T. Biedron and David L. Whitaker**
Analytical Services and Materials, Inc.
Hampton, Virginia

** Currently with Cray Research, Inc., Eagan, Minnesota*

High-Alpha Projects & Technology Conference - DFRC

Background

At high angles of attack, vortical flows play a crucial role in the maintenance of lift for fighter aircraft. However, under certain conditions, the vortical flow can have an adverse effect on the aircraft. On the F/A-18 the LEX vortex can impinge on the tail; at high angles of attack the unsteady flow from vortex bursting can cause structural fatigue on the vertical tails.

At high angles of attack, the flow field can be quite complex, and a computational analysis challenging. A full configuration analysis with viscous structured grids can be computationally expensive and the task of generating the requisite grids can be quite difficult. To mitigate these difficulties and provide a medium-fidelity analysis tool, a hybrid structured/unstructured approach was adopted for this work. In this analysis, the formation and roll-up of the LEX vortex is computed with a structured Navier-Stokes solver, and the resulting vortex propagated downstream with an unstructured Euler solver.

Background

- ***Motivation: Analysis of vortex-tail interaction***
  - ***At high alpha, LEX vortex impinges on tail, causing structural fatigue***
  - ***Full configuration analysis with viscous structured grid computationally expensive; grid generation difficult***
- ***Adopt a hybrid structured/unstructured approach***
  - ***Model formation and roll-up of vortex with structured NS solution on forebody/LEX***
  - ***Propagate vortex to tail with unstructured Euler solution over remainder of aircraft***

F/A - 18 Hybrid Grid System, Symmetry Plane

The figure shows the symmetry-plane grids of the structured/unstructured hybrid-grid system. The structured zone consists of four blocks, with patched-grid interfaces between blocks (block faces lie on a common surface, but points do not match). The unstructured zone consists of tetrahedra. There is a small amount of overlap between the structured and the unstructured zones, with the overlap occurring near FS 345.

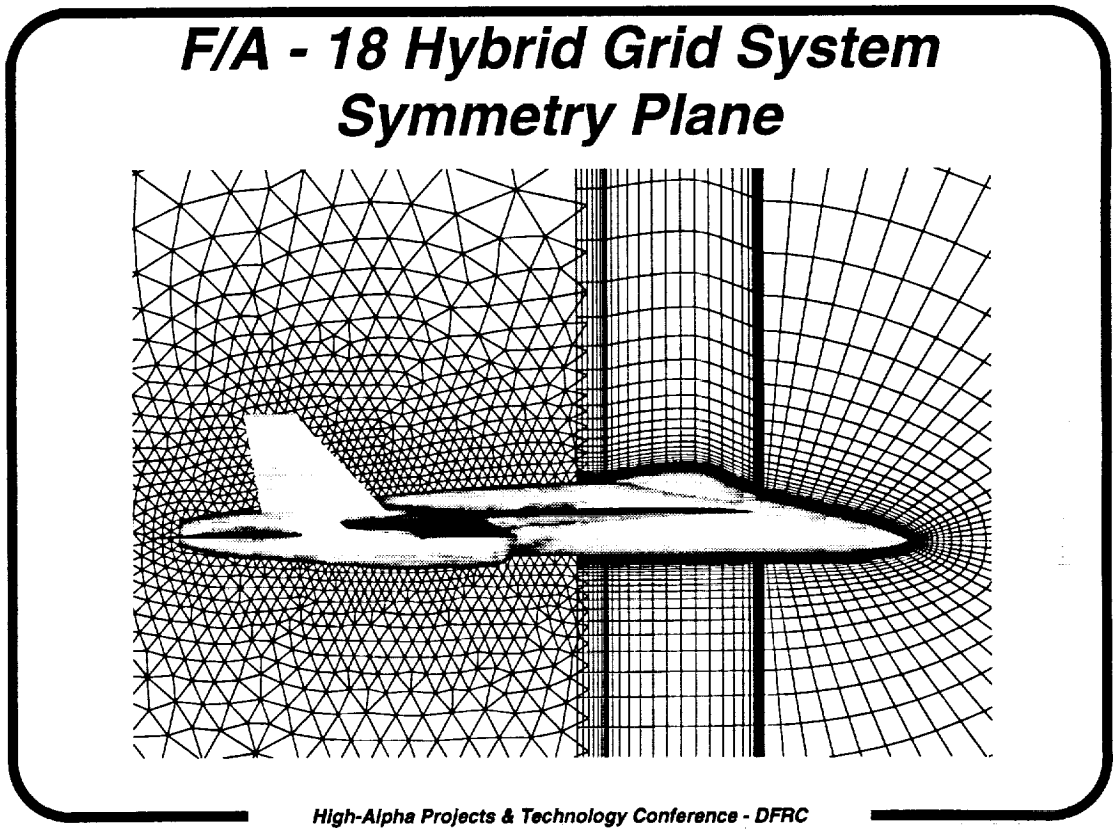

Methodology

Two flow solvers were used in this analysis: CFL3D for the structured, viscous zone and UNS3D for the unstructured Euler zone. Both codes are upwind, finite-volume schemes. CFL3D is cell-center based whereas UNS3D is node based. Communication between the structured and unstructured zones is obtained via a common overlap region, near station 345 (aft of the canopy). A modified "chimera" scheme is used to transfer data between the zones: volume-weighted interpolation is used to transfer data from the unstructured zone to the structured zone, while tri-linear interpolation is used to transfer data from the structured zone to the unstructured zone.

Methodology

- *Flow solvers*
  - *CFL3D for structured viscous zone*
    - *Upwind, finite-volume; cell-center based*
  - *UNS3D for unstructured Euler zone*
    - *Upwind, finite-volume; node based*
- *Communication between zones via common overlap region, near FS 345 (aft of canopy)*
  - *Volume-weighted interpolation from unstructured zone to structured zone*
  - *Tri-linear interpolation from structured zone to unstructured zone*

Solutions

Solutions have been obtained for three angles of attack: 19, 26 and 30 degrees. Data from the HARV are available at these angles-of-attack for comparison with the computed solutions. The solutions are obtained with local time stepping, that is they are not time accurate. The solutions are obtained as follows. A fixed number of iterations are run in the viscous zone, after which data is transferred to the unstructured zone. A fixed number of iterations is then performed in the unstructured zone, followed by data transfer to the structured zone. This process completes one global iteration. For the results presented here, 10 iterations were used in each zone. Solutions require on the order of 100 global iterations, translating into approximately 10 hours on a Cray YMP.

The structured forebody grid system consisted of 4 blocks, with a total of approximately 250,000 cells. The unstructured zone over the aft end of the aircraft consisted of approximately 90,000 nodes forming approximately 495,000 tetrahedra. In the structured zone, the number of unknowns to be solved for is proportional to the number of cells is, whereas in the unstructured zone, the number of unknowns is proportional to the number of nodes

Solutions

- ***Solutions obtained for*** $\alpha = 19°$, $\alpha = 26°$, ***and*** $\alpha = 30°$ ***with local time stepping***
  - ***Fixed number of iterations in each zone (~10) comprises 1 global iteration***
  - ***Solutions require ~100 global iterations***
  - ***Total solution time ~10 hours on Cray YMP***
- ***Composite grid statistics***
  - ***Forebody (structured) grid comprised of 4 blocks with a total of 250,000 cells***
  - ***Aft (unstructured) grid comprised of a single block with 90,000 nodes (495,000 tetrahedra)***

F/A - 18 HARV Pressure Data Stations

The figure shows a layout of the locations at which pressure data were taken during HARV flight tests. Computed pressures will be shown at the same stations. The figure also illustrates the format in which the data is presented. On the forebody, pressures are given versus theta, the angle measured from bottom dead center. On the LEX, data are given versus the dimensionless LEX span. The cross section identifier "BB" happens to be positioned at the approximate location of the zonal interface between the structured and the unstructured computational zones.

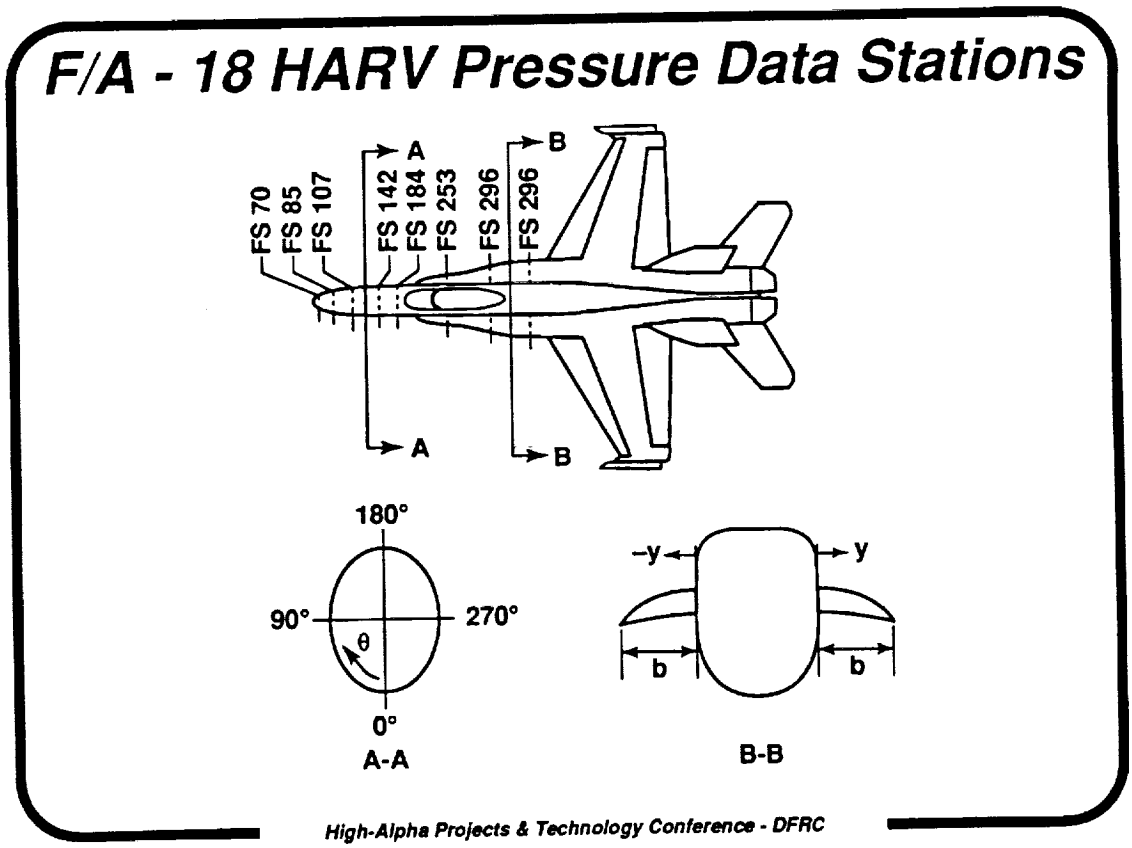

Forebody Pressure Coefficients, Alpha = 19 ^{o}

The figure shows the computed pressure coefficients on the forebody surface for an angle of attack of 19°. The agreement between the computation and the flight data is generally good. It should be noted that at FS 142, near θ= 90° and θ= 270°, the HARV pressure distribution exhibits a local suction peak not captured in the computed results. This is because a pair of antenna fairings, present on the HARV, are not modeled in the computational geometry.

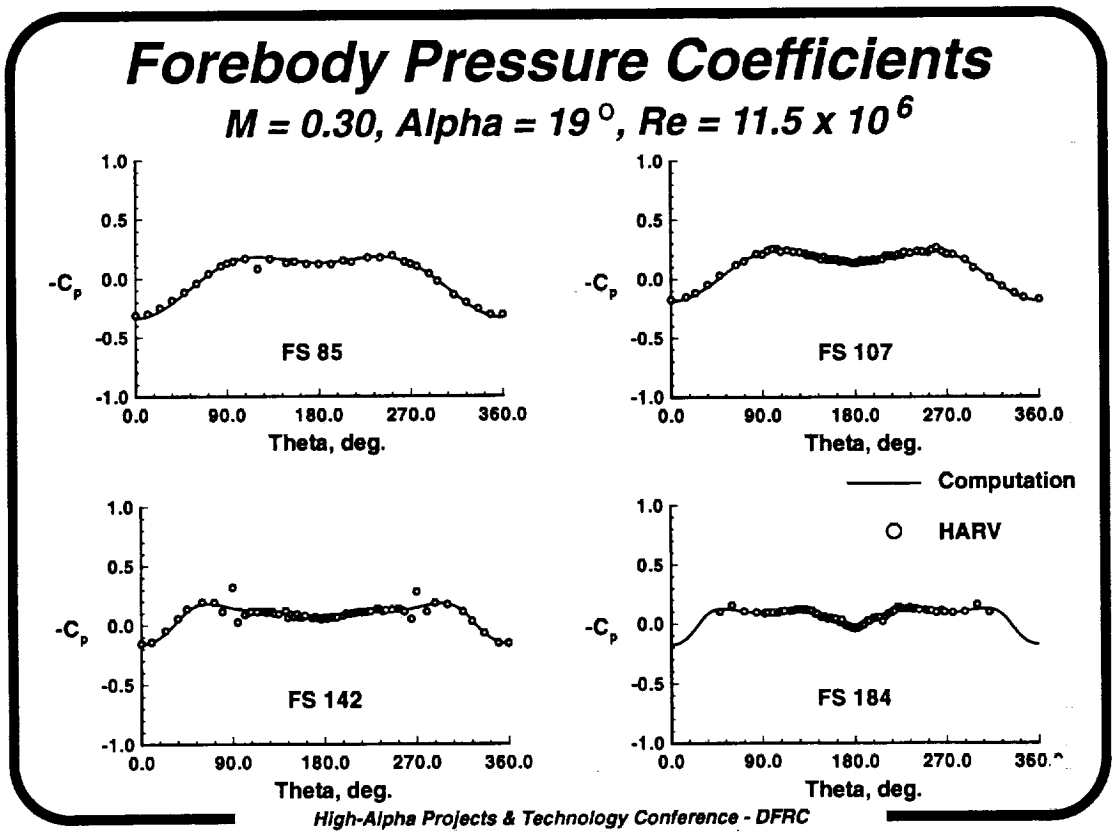

LEX Pressure Coefficients, Alpha = 19 °

The figure shows the computed pressure coefficients on the LEX surface for an angle of attack of 19°. The agreement between the computation and the flight data is generally quite good. Stations FS 253 and FS 296 lie inside the structured computational zone, while station FS 357 lies inside the unstructured computational zone. The coarser spanwise spacing in the unstructured zone is apparent, although the primary features - the footprint of the primary LEX vortex near y/b = 0.5 and the footprint of the secondary vortex near y/b = 0.9 - are predicted reasonably well.

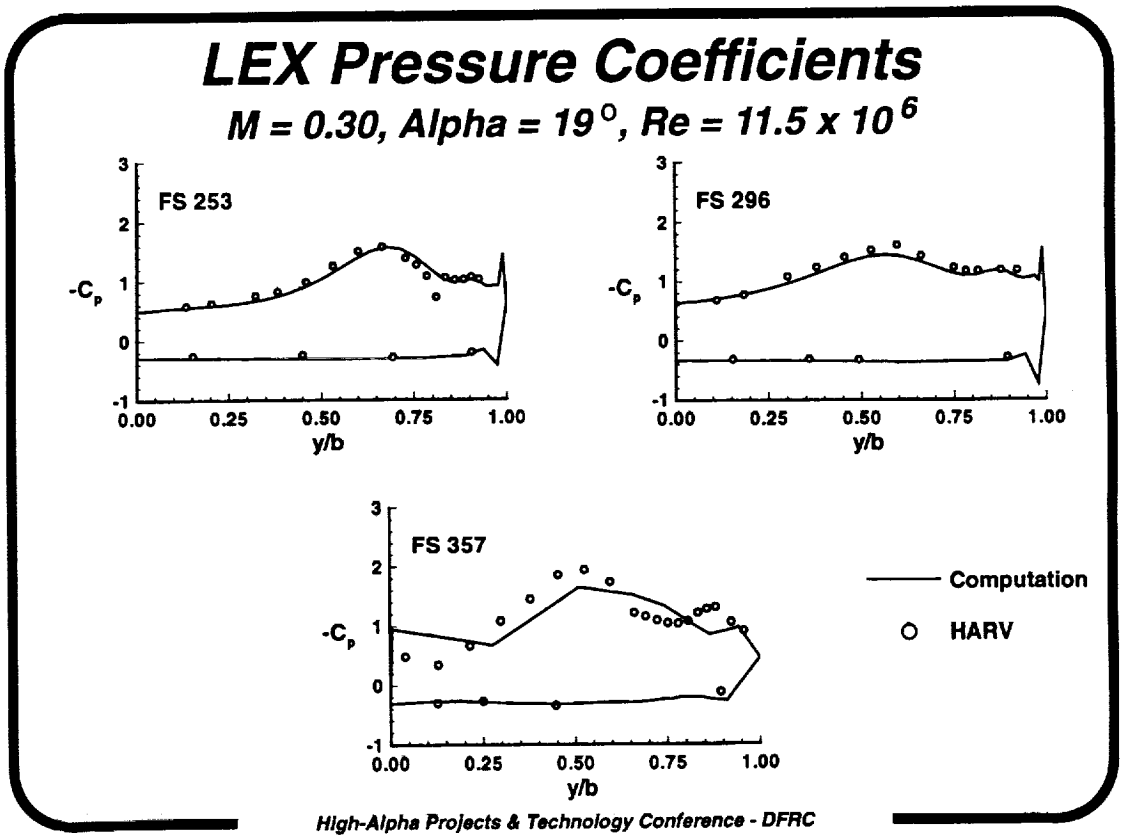

LEX Vortex, Alpha = 19 °

The figure shows the computed streamline traces following the LEX vortex core for an angle of attack of 19°. The particles were released near the apex of the LEX. The computed vortex shows no sign of bursting at this angle of attack. In contrast, data from the HARV indicates that the vortex bursts at a streamwise position corresponding to the intersection of the leading edge of the vertical tail and the fuselage.

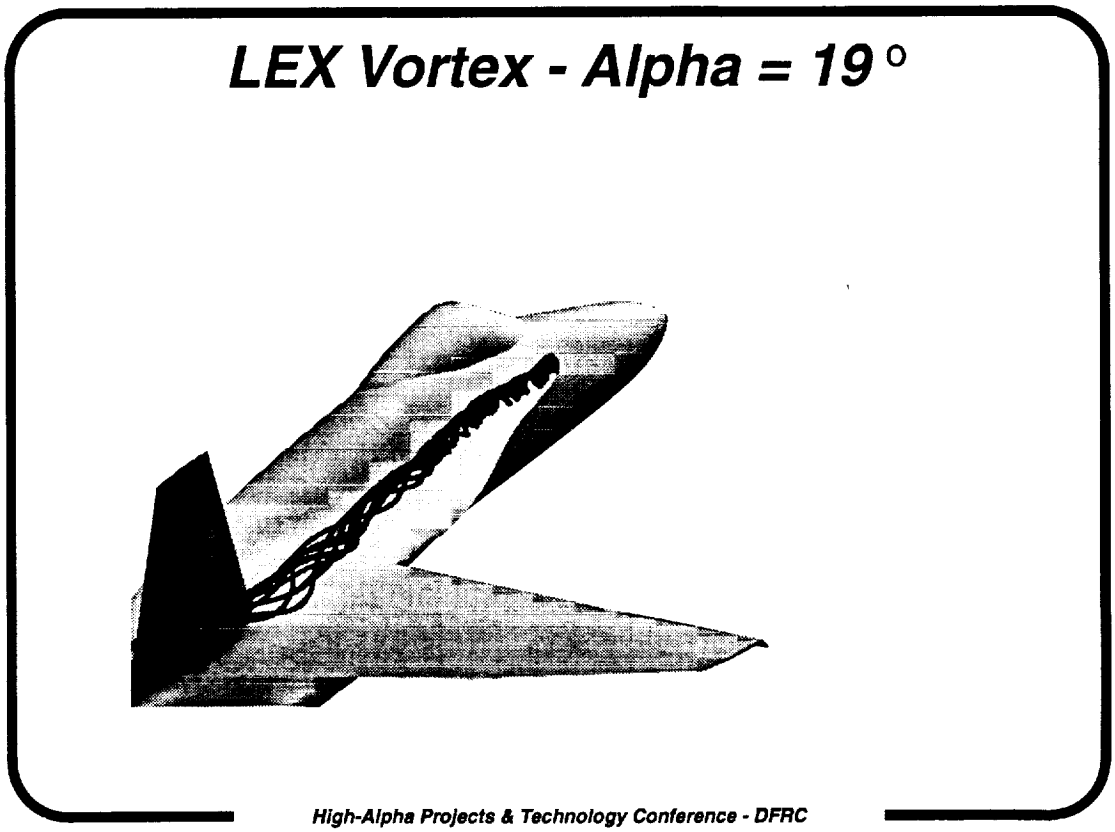

Forebody Pressure Coefficients, Alpha = 25.8 °

The figure shows the computed pressure coefficients on the forebody surface for an angle of attack of 25.8°. The agreement between the computation and the flight data is again generally good.

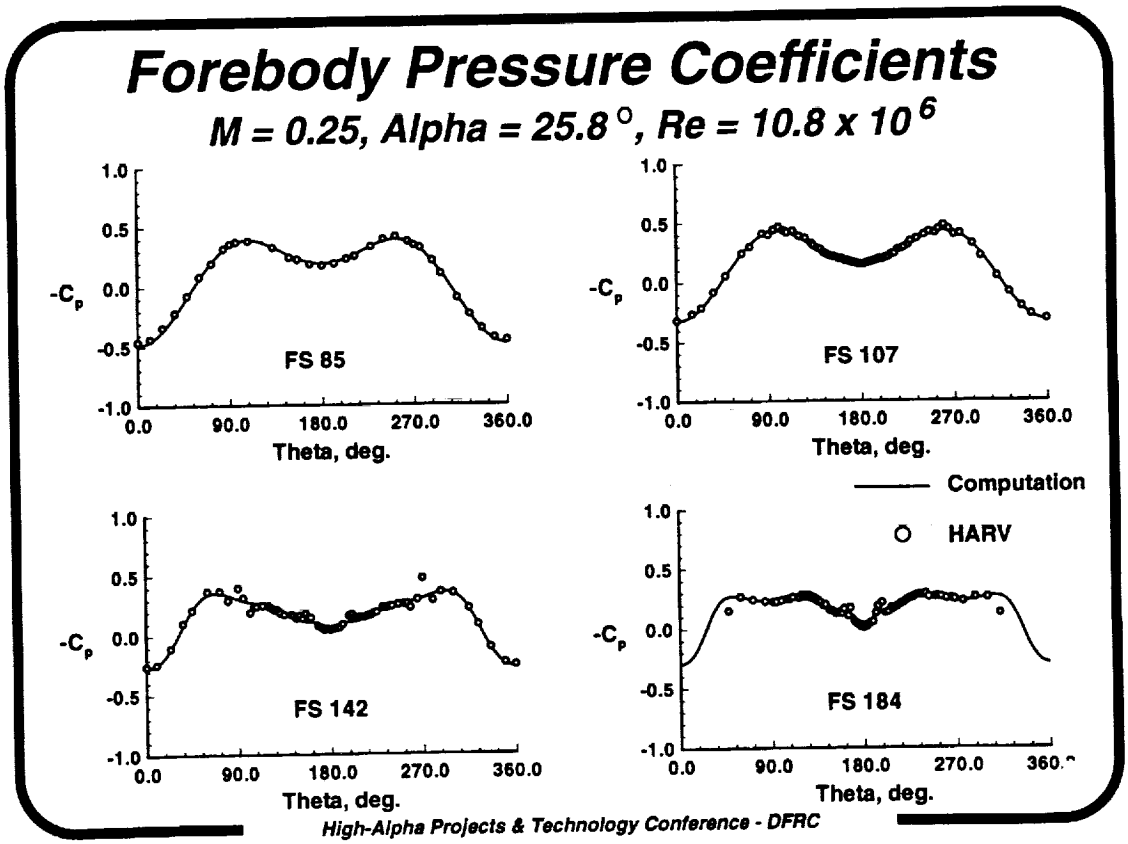

LEX Pressure Coefficients, Alpha = 25.8 °

The figure shows the computed pressure coefficients on the LEX surface for an angle of attack of 25.8°. The agreement between the computation and the flight data is quite good. Compared to 19°, the LEX vortex is stronger at all three stations, as indicated by increased suction on the upper surface of the LEX.

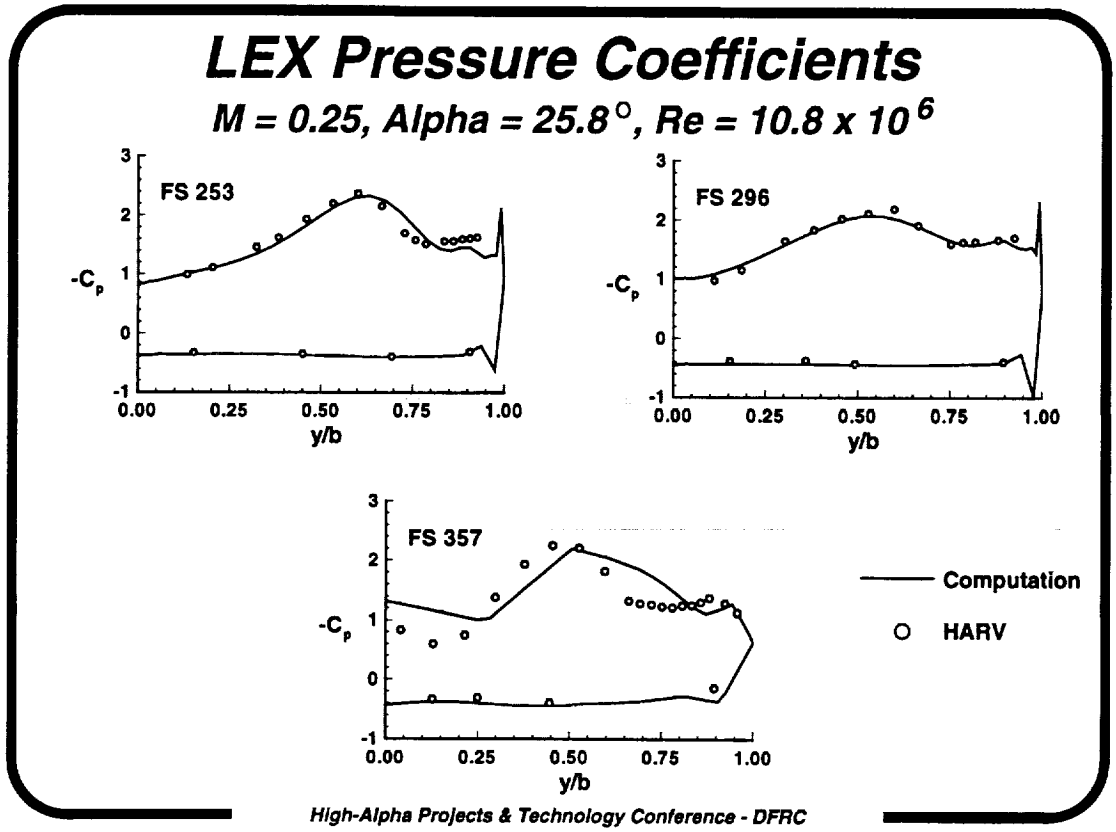

LEX Vortex, Alpha = 26 °

The figure shows the computed streamline traces following the LEX vortex core for an angle of attack of 25.8°. The particles were released near the apex of the LEX. For this angle of attack, the computed vortex exhibits a sudden expansion of the core, indicative of burst. In addition, the axial velocity in the vortex core becomes negative at a point slightly downstream of the region in which the core begins to expand. If the burst point is defined as the location at which the axial velocity in the core first becomes negative, then the computed results predict bursting at FS 535, or X/L = 0.7, where L is the length of the aircraft. The burst position observed in flight is given in published reports (AIAA-90-0231) as approximately X/L = 0.52.

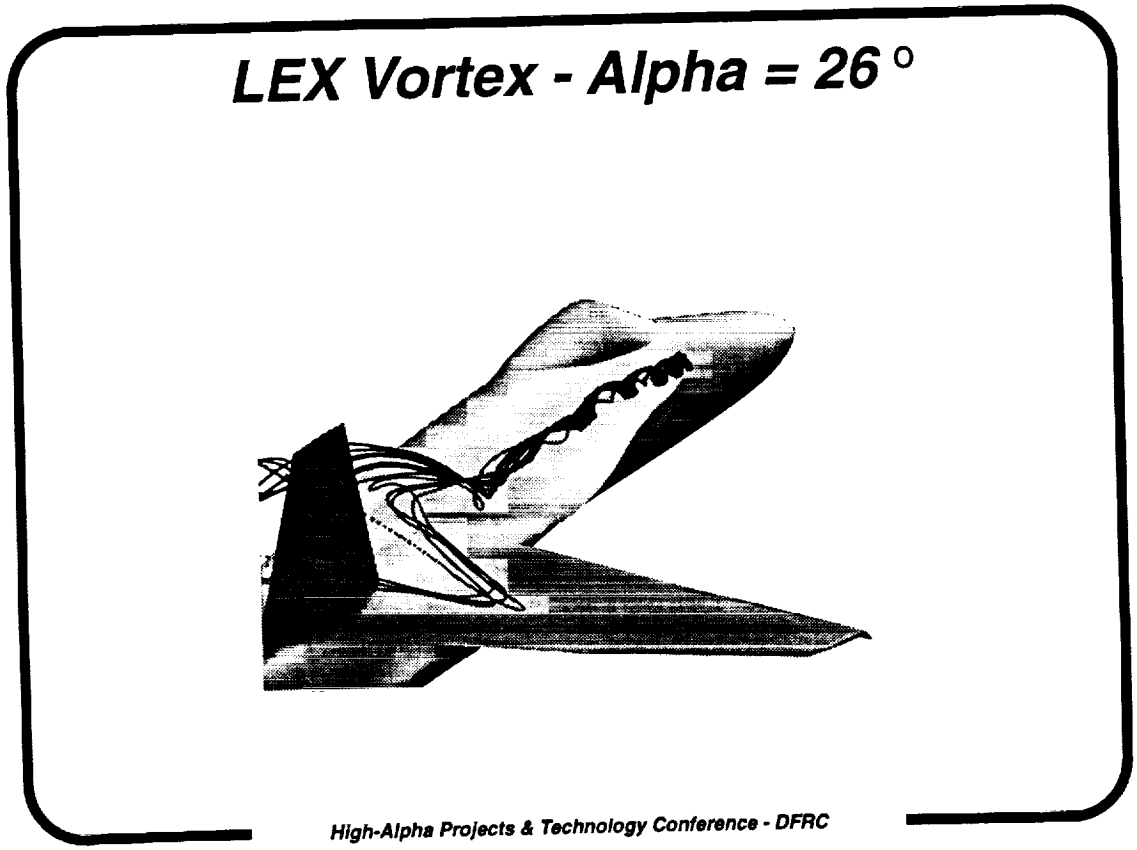

LEX Vortex and Surface-Pressure Contours, Alpha = 26 ^{o}

The figure shows the both the computed streamline traces following the LEX vortex core and surface pressure contours for an angle of attack of 25.8°. The computed results, obtained for conditions of zero yaw, were reflected about the vertical plane of symmetry to produce the view shown here. The vortex trace was omitted from the reflected half in order to better show the pressure contours on the LEX.

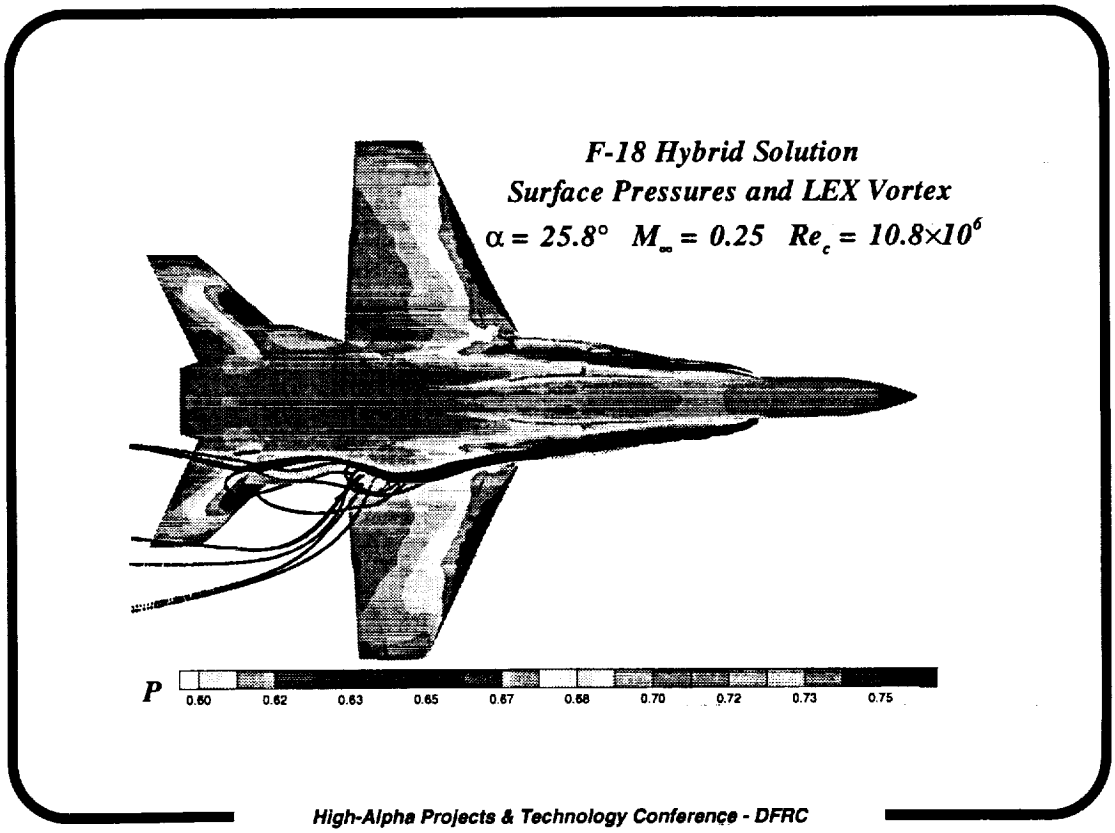

Forebody Pressure Coefficients, Alpha = 30 °

The figure shows the computed pressure coefficients on the forebody surface for an angle of attack of 30°. The agreement between the computation and the flight data is generally good, although the footprint of the forebody vortex - seen as the local suction peak on either side of θ = 180° - is underpredicted. The footprint is not observed in the computational results until FS 142, whereas in the HARV data the footprint is evident as far forward as FS 107. This is likely due to insufficient circumferential resolution near the top of the forebody.

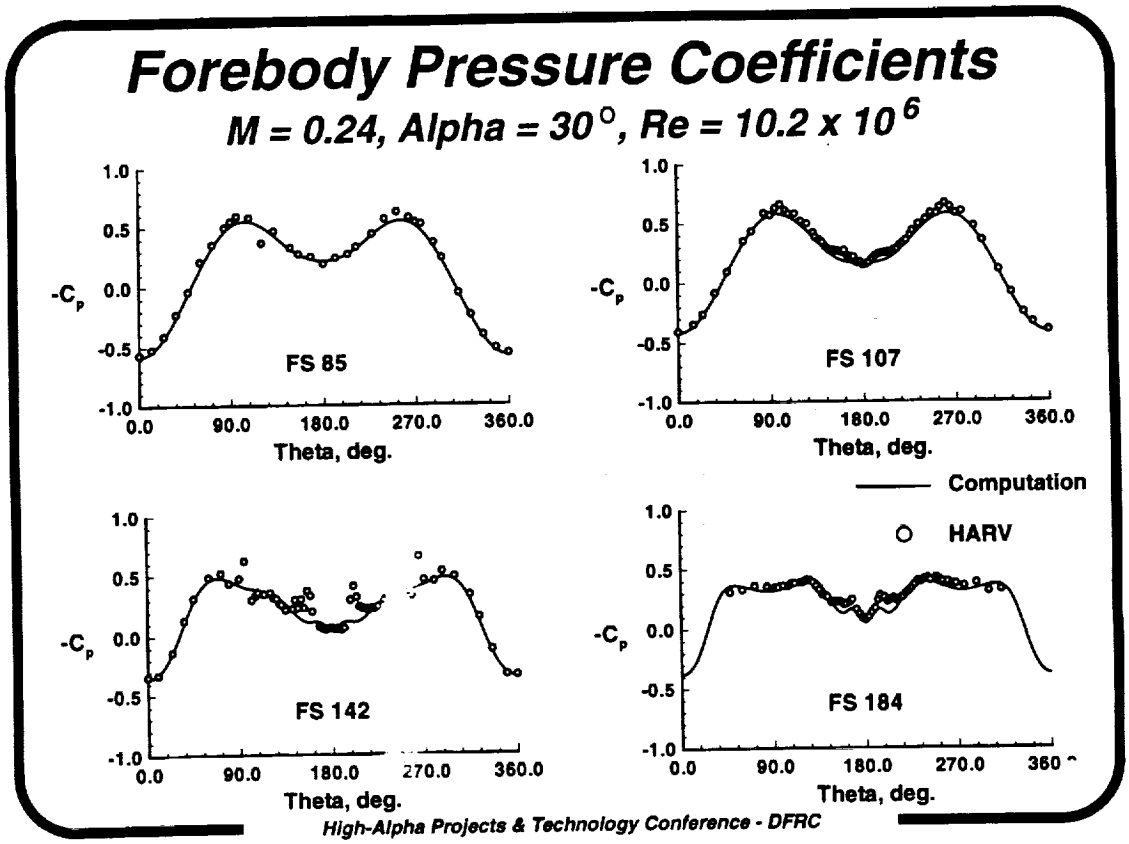

LEX Pressure Coefficients, Alpha = 30 ^{o}

The figure shows the computed pressure coefficients on the LEX surface for an angle of attack of 30°. The peak suction pressure has increased at both FS 253 and FS 296, compared to the corresponding suction pressures at an angle of attack of 26°. However, the suction level at FS 357 remains essentially unchanged from the alpha = 26° case, and is observed in the flight data as well. Interestingly, although the flight-test burst point given in AIAA-90-0231 for alpha = 30° is X/L = 0.42, corresponding to FS 333, no loss of suction pressure is observed at FS 357. The computed vortex burst point, as defined as the point where the core axial velocity first becomes negative, is X/L = 0.68 (FS 502).

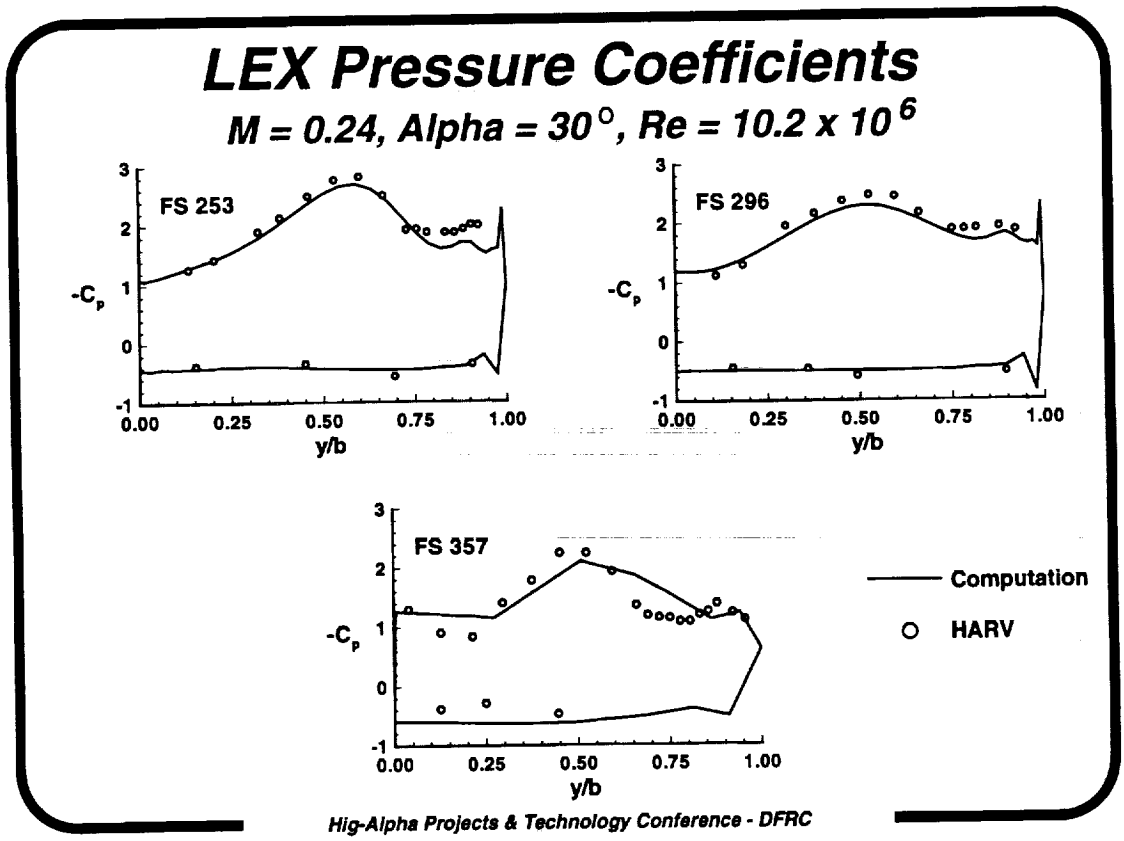

LEX Vortex, Alpha = 30 °

The figure shows the computed streamline traces following the LEX vortex core for an angle of attack of 30°. As at alpha = 26°, the computed vortex exhibits the characteristics of a burst vortex, with a burst point at X/L = 0.68.

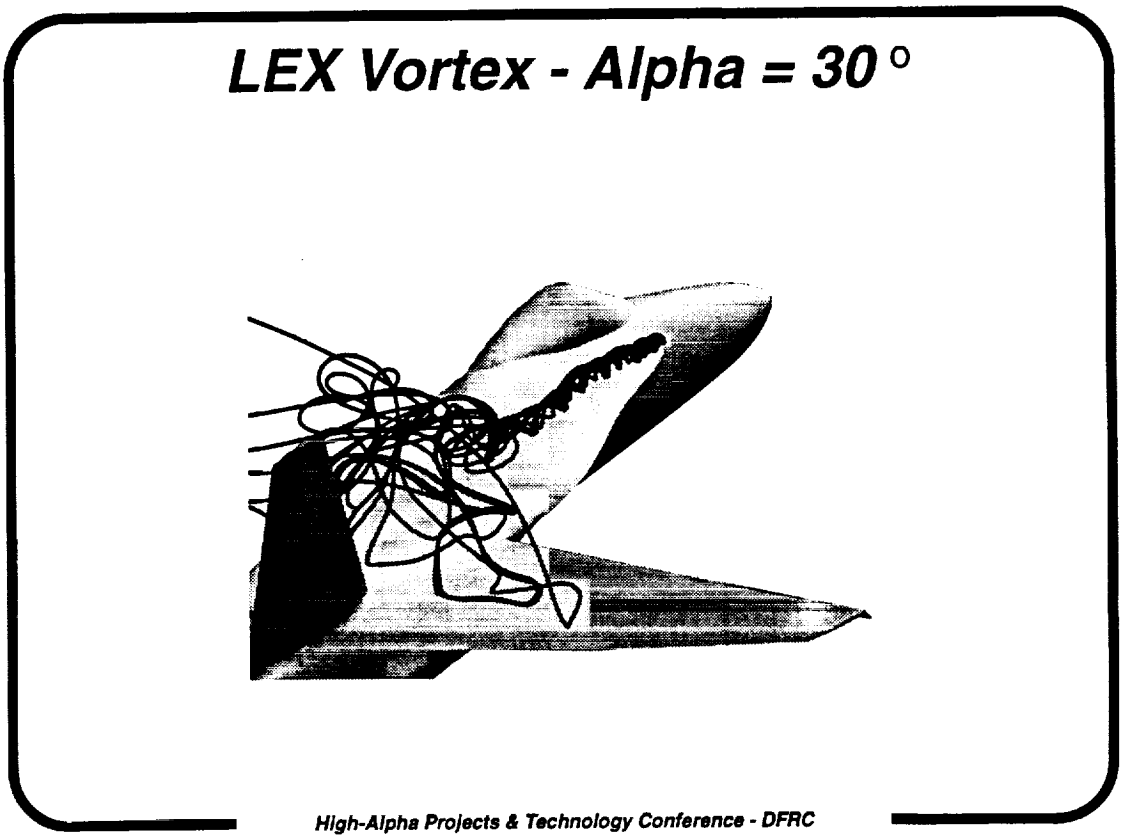

SUMMARY

A methodology for coupling a structured, Navier-Stokes code to an unstructured Euler code has been developed and applied to the F/A - 18 at high angle of attack. The hybrid code has been used to compute flows at 19, 26 and 30 degrees angle of attack. The computed pressure distributions show generally good agreement with the HARV flight test data, particularly on the LEX surface. No vortex burst was predicted at 19 degrees. The predicted burst points for the two higher angles of attack were in qualitative agreement with flight-test observations, with the burst points located downstream of those observed in flight. A grid refinement study is necessary to assess the effect grid density has on the computed burst locations.

Summary

- ***Developed methodology for coupling structured, Navier-Stokes code to unstructured Euler code***
- ***Hybrid code used to compute flows at*** $\alpha = 19°$, $\alpha = 26°$ ***, and*** $\alpha = 30°$
- ***Computed LEX pressures in good agreement with HARV flight data***
- ***Burst predicted at*** $\alpha = 26°$ ***and*** $\alpha = 30°$ ***, but not at*** $\alpha = 19°$***; bursting, when predicted, occurs downstream of the location observed in flight***
- ***Grid refinement necessary to assess the effect on burst location***